Supplementary Information

The anion-π^+ interaction strategy enhances PDT antibacterial performance of AIE-active photosensitizers

Ying Zhang,[a] Renmanduhu Sha,[a] Jianye Gong,[a] Lingxiu Liu,[a] Lina Feng,[a] Weijing Zhang,[b] Guoyu Jiang*[a] and Jianguo Wang*[a]

[a] College of Chemistry and Chemical Engineering, Institute of Green Chemistry and Environment, Institutes of Biomedical Sciences, Inner Mongolia Key Laboratory of Synthesis and Application of Organic Functional Molecules, Inner Mongolia University, Hohhot 010021, P. R. China.

E-mail: jiangguoyu@mail.ipc.ac.cn, wangjg@iccas.ac.cn

[b] Xi'an Modern Chemistry Research Institute, Xi'an 710069, P. R. China.

Experimental Procedures

Materials

Phosphate buffered solution (PBS, pH 7.4), 2',7'-dichlorodihydrofluorescein diacetate (DCFH-DA), aminophenyl fluorescein (APF), hydroxyphenyl fluorescein (HPF), dihydrorhodamine 123 (DHR123), 9,10-anthracenediylbis(methylene) dimalonic acid (ABDA), calcein acetoxymethyl ester (Calcein-AM), propidium iodide (PI) were purchased from Sigma-Aldrich. Thiazolyl blue tetrazolium bromide (MTT) was purchased from Beyotime biotechnology Co., Ltd. All other chemicals and reagents were purchased from Admas-beta® and used directly without further purification. *S. aureus* (BNCC 186335) and methicillin-resistant *S. aureus* (MRSA) (BNCC 337371) were purchased from BeNa Culture Collection. *E. coli* was obtained from the Engineering Research Center of Dairy Quality and Safety Control Technology, Ministry of Education, Inner Mongolia University.

Instruments

^{1}H and ^{13}C NMR spectra were recorded with Bruker ARX 500 NMR or Bruker ARX 600 NMR spectrometer using tetramethylsilane (TMS) as a reference. High resolution mass spectra (HRMS) were measured with a LCMS9030 spectrometer. Single crystal X-ray diffraction was performed on a Rigaku Oxford Diffraction Supernova Dual Source, Cu at Zero equipped with an AtlasS2 CCD using Cu Kα radiation. Absorption spectra were measured on a SHIMADZU UV-2600i spectrophotometer. Photoluminescence (PL) spectra were recorded on a HITACHI F-4700 spectrophotometer. For MTT assay, the absorbance of each sample was measured using a microplate reader (BioTek). The bacterial imaging experiments were performed with inverted fluorescence microscope (Nikon Ti2). The bacterial morphology was observed on a HITACHI S-4800 scanning electron microscope. The photographs of agar plate were taken by an automated colony counter (Shineso Icount33). In antibacterial assay, a CEL-PF300-T8 solar stimulator was used as the light source equipped with a 400 nm cut-off filter to remove the short wavelength light. The light power density was maintained at 100 $mW \cdot cm^{-2}$ during irradiation.

Density functional theory calculations

The molecular orbital amplitude plots of HOMOs and LUMOs of DTPAP, DTPAP-Br and DTPAP-2Br were calculated based on their single crystal structures at the level of B3LYP/6-31G (d,p)[S1]. The density functional theory (DFT) method was used to optimize geometries of DTPAP, DTPAP-B and DTPAP-2B at the level of M062X[S2]/6-311g(d) within Gaussian 09 Package[S3]. The excited energies and SOCs between singlet and triplet states were calculated by the time-dependent density functional theory (TD-DFT) method at the same level within ORCA 4.0 Package[S4]. The independent gradient model (IGM) analysis of weak interaction based on single crystal structure was conducted by using Multiwfn program. The corresponding structure and IGM isosurfaces were generated using visual molecular dynamics (VMD) program[S5]. The electrostatic potential (ESP)

characteristic parameters were calculated based on the single crystal structure with electronic wave function information using Multiwfn. The visualization of the ESP distribution was performed using GaussView 6.0. The anion-π^+ interaction energies were calculated by single-point calculations using the M062X/6-311g(d) method according to the equation $E = E_{complex} - E_{anion} - E_{cation}$, where E = anion-π^+ interaction energy, $E_{complex}$ = the energy of DTPAP-2B, E_{anion} = the energy of anion, E_{cation} = the energy of cation.

Single crystal X-ray structure analysis

Three suitable single crystals of the three compounds were selected and mounted on a Rigaku SuperNova, Dual, Cu at zero, AtlasS2 diffractometer (Kα monochromator, CCD area detector). The diffraction intensities data were collected at 120.0, 153.2 and 220.0 K for DTPAP, DTPAP-B, and DTPAP-2B, respectively. Multi-scan absorption corrections and data reductions were applied using *CrysAlisPro 1.171.38.43f* (Rigaku Oxford Diffraction, 2015).[S6] The initial structures were solved by Direct Methods using *SHELXS*,[S7] and the coordinates of the rest of the non-H atoms were obtained from difference Fourier maps. All coordinates and anisotropic thermal parameters of the non-H atoms were refined by full-matrix least-squares techniques based on F^2 using *SHELXL*[S8] within *Olex2*[S9-S10] interface. The masked solvent molecules were also explored by *Olex2* (no valid masked solvent molecules were explored in DTPAP, two $CH_3COOC_2H_5$ and three CH_3OH molecules were explored in an asymmetric unit of DTPAP-B and DTPAP-2B, respectively). All coordinates of H atoms were obtained by geometry methods and their positions and isotropic thermal parameters were constrained. Several very central C, N, and H atoms and the electron-countered Br^- anions in DTPAP-B were treated as disordered, their site occupancies were refined.

Total ROS detection by DCFH

A commonly used ROS indicator 2',7'-dichlorodihydrofluorescein diacetate (DCFH-DA) was applied to detect the ROS generation of DTPAP, DTPAP-B and DTPAP-2B in PBS under white light irradiation (10 mW cm^{-2}). Briefly, 0.5 mL DCFH-DA in ethanol (1 mM) was added to 2 mL NaOH (10 mM) and allowed to be stirred at room temperature for 30 min. Then the hydrolysate was neutralized with 10 mL PBS, and kept in dark until use. By the time, DCFH-DA was hydrolyzed to 2',7'-dichlorofluorescein (DCFH). Then DCFH (40 μM) in PBS was further diluted to 1 μM in the sample solution of RB, DTPAP, DTPAP-B or DTPAP-2B (0.25 μM) for measurement by PL instrument. The fluorescence of DCFH triggered by PSs sensitized ROS under white light irradiation was recorded at different time intervals. The PL spectra were measured with excitation at 489 nm and emission was collected from 500 to 600 nm. The fluorescence intensity at 523 nm was used to indicate the total ROS generation rate of RB, DTPAP, DTPAP-B or DTPAP-2B.

Detection of $O_2^{\bullet-}$ generation by DHR123

Compound DHR123 was used as indicator for detection of $O_2^{\bullet-}$ in solution. When $O_2^{\bullet-}$ is generated in the system, DHR123 will be oxidized to emit strong fluorescence at 530 nm. 0.25 μM of DTPAP, DTPAP-B or DTPAP-2B were dissolved in 2 mL PBS containing 5 μM of DHR123. The mixture was then placed in a cuvette and irradiated by white light irradiation (10 mW cm^{-2}). The fluorescence

changes of sample at 530 nm were recorded by the PL spectrofluorometer (Excitation wavelength: 480 nm).

Detection of •OH generation by HPF

Compound HPF was used as indicator for detection of •OH in solution. When •OH is generated in the system, HPF will be oxidized to emit strong fluorescence at 515 nm. 0.25 μM of DTPAP, DTPAP-B or DTPAP-2B were dissolved in 2 mL PBS containing 5 μM of HPF. The mixture was then placed in a cuvette and irradiated by white light irradiation (10 mW cm^{-2}). The fluorescence changes of sample at 515 nm were recorded by the PL spectrofluorometer (Excitation wavelength: 490 nm).

Detection of $^1O_2$ generation by ABDA

$^1O_2$ generation in solution was monitored with ABDA as the indicator. Briefly, ABDA in DMSO (working concentration: 50 μM) was mixed with the DTPAP, DTPAP-B or DTPAP-2B (working concentration: 0.25 μM) and irradiated by white light irradiation (10 mW cm^{-2}). Then, the absorbance of ABDA at 325-425 nm was recorded for every five seconds.

Bacteria culture

A single colony of *S. aureus*, MRSA or *E. coli* on LB agar was transferred to 10 mL of LB liquid culture and grown for 10 h at 37 ℃ with a shaking speed of 220 rpm. Bacteria were harvested by centrifuging at 4000 rpm for 7 min and washed twice with PBS. After removal of the supernatant, the remaining bacteria were resuspended in PBS, and diluted to an optical density of 1.0 at 600 nm (OD600 = 1.0 with about 10^9 CFU mL^{-1}).

Antimicrobial assay

Bacteria (*S. aureus*, *E. coli* or MRSA) at a density of ~10^7 CFU mL^{-1} were dispersed in the solutions containing PSs (0, 0.05, 0.1, 0.2, 0.4, 0.6 and 0.8 μM). These mixed solutions were then incubated at 37 °C with a shaking speed of 220 rpm for 15 min. Next, the bacterial suspensions were exposed to white light irradiation for 15 min (100 mW cm^{-2}) for phototoxicity test or were further incubated in darkness at 37 ℃ for assessing the dark toxicity. Afterward, the samples were diluted to a density of ~10^2 CFU mL^{-1} with PBS and spread on the LB agar plate, followed by culturing at 37 °C for 16 h before CFU counting and taking photos.

SEM analysis

Followed by antimicrobial experiments, the bacteria were collected after irradiation and fixed with 2.5% glutaraldehyde overnight. The glutaraldehyde was removed by centrifugation and the bacteria were washed with PBS for 2 times. Then the bacteria were dehydrated with a series of graded ethanol/water solution (*v*ethanol%=10%, 30%, 50%, 70%, 80% 90%, 100%) for 15 min. 2 μL of bacterial suspensions was added onto clean silicon slices followed by naturally drying in the air. The specimens were coated with Au before SEM analysis.

Live/dead staining assay

Followed by antimicrobial experiments, the bacteria were collected after irradiation and incubated with Calcein-AM (10 μM) and PI (10 μM) for 1 h. Then, the bacteria were washed one time with sterile PBS. The resulting bacterial suspension (2 μL) was added onto a glass slide, which was immobilized by a clean coverslip for characterization by inverted fluorescence microscope. Excitation wavelength: 426-466 nm for Calcein-AM, 500-550 nm for PI, emission filter: 511-551 nm for Calcein-AM, 573-613 nm for PI.

Zeta potential measurements

S. aureus or MRSA at a density of ~10^8 CFU mL^{-1} were incubated with PSs (50 μM) at 37 °C with a shaking speed of 220 rpm for 5 min, respectively. The bacteria were harvested by centrifugation at 4000 rpm for 7 min and dispersed in PBS for zeta potential measurements. As for negative controls, bacterial without PSs were treated under the same conditions.

Cell culture

NIH3T3 cells were cultured in DMEM (containing 10% heat-inactivated FBS, 100 mg mL^{-1} penicillin and 100 mg mL^{-1} streptomycin) at 37 °C in a humidified incubator with 5% CO_2. Before the experiments, the cells were precultured until confluence was reached.

Cell viability via MTT assay

100 μL of LO2 cell suspension (5000 cells/well) was uniformly distributed in a 96-well plate. The cells were pre-incubated for 24 h at 37 ℃ in a humidified incubator. Remove old media and then add 100 μL fresh medium containing various concentrations of PSs (0 μM, 0.05 μM, 0.1 μM, 0.2 μM, 0.4 μM, 0.6 μM, 0.8 μM) to the plate. After co-incubating the plate for 20 h in a humidified incubator, the plate was exposed to white light irradiation (100 mW cm^{-2}) for 15 min and cells without any treatment in darkness were used as dark group. The plate was normally nurtured for another 4 h at 37 ℃. Subsequently, the serum-containing media was replaced with serum free media and MTT reagent in cell cultures for 4 h, followed by the addition of 100 μL of DMSO to dissolve the formazan crystals. Absorbance was taken at 490 nm by a microplate reader (Biotek). The cells incubated with a culture medium was used as a control. All the experiments were performed in triplicate. The results were expressed as the viable percentage of cells after different treatments relative to the control cells without any treatment. The relative cell viability was calculated according to the following formula: Cell viability (%) = $(OD_{sample} - OD_{background})/(OD_{control} - OD_{background}) \times 100\%$.

***In vivo* assay against MRSA**

BALB/c mice (6−8 weeks old, average body weight 16−18 g) were purchased from SPF Biotechnology Co., Ltd. (Beijing, China) and all animals received care in compliance with the guidelines outlined in the Guide for the Care and Use of Laboratory Animals. All procedures were

approved by the Institutional Animal Care and Use Committee at the Inner Mongolia University (IMU-2023-mouse-017). The mice were randomly divided into four groups: MRSA-infected wound treated with (1) PBS in darkness (PBS+D); (2) PBS plus white light irradiation treatment (PBS+L); (3) DTPAP-2B in darkness (DTPAP-2B+D); (4) DTPAP-2B plus white light irradiation treatment (DTPAP-2B+L). The mice were anesthetized by injection of 1% pentobarbital sodium saline solution (5 mL·kg^{-1}), and hair removal cream was used to remove the hair on their backs for subsequent experiments. Next, a full-thickness skin wound with a diameter of 8 mm was made on the back of each mouse. Bacterial suspension (100 μL, 1×10^8 CFU mL^{-1}) was dripped on the surface of wounds, and the bacterial suspension were kept in the wounds for 30 minutes. Thirty minutes later, 50 μL of PBS or DTPAP-2B (0.8 μM) was sprayed on infected wounds for another 15 min, and treated with or without white light irradiation (100 mW cm^{-2}) for 15 min. In sterile environment, mice were fed separately in different cages to facilitate wound healing after operation. The wound sizes were imaged by a video camera and calculated at designated time intervals.

Histological analysis

The wounds were histologically analyzed at day 11 post operation. Wound tissues were collected and fixed in 4% formaldehyde solution for 30 min. The pathological sections of wound tissues were analyzed by H&E staining. Histological images were taken by an inverted microscopy.

Biosafety assessment

To further evaluate the safety of different treatments *in vivo*, blood samples were collected from mice with various treatments for complete blood panel analysis. White blood cell (WBC) counts, lymphocyte counts (LYMPH#), neutrophil counts (NEUT#), red blood cell (RBC), hemoglobin (HGB), and platelets (PLT) were measured.

Hemocompatibility test

Whole blood was collected from healthy mice (2000 rpm, 10 min). PBS was used to wash the obtained erythrocytes for three times. Subsequently, 50 μL of blood cells were treated with varying concentrations of DTPAP-2B (0.05, 0.1, 0.2, 0.4, 0.6, 0.8, 1 μM) in polyethylene pipe containing 1 mL of PBS, and incubated for 2 h at 37 ℃. PBS and 1% Triton X-100 (Triton) were used as negative control and positive control, respectively. Then, all samples were centrifuged for 10 min, and images were captured. The absorbance of the supernatant was measured at 540 nm. To correct for compound absorbance, DTPAP-2B in PBS solution with the same concentration was used as the blank group. Hemolysis was calculated using the following formula:

$$\text{Hemolysis (\%)} = \frac{A_{Blood} - A_{Sample}}{A_{Triton} - A_{PBS}} \times 100\%$$

Synthesis and characterization

DTPAP was easily synthesized according to the previous reported literature [S11].

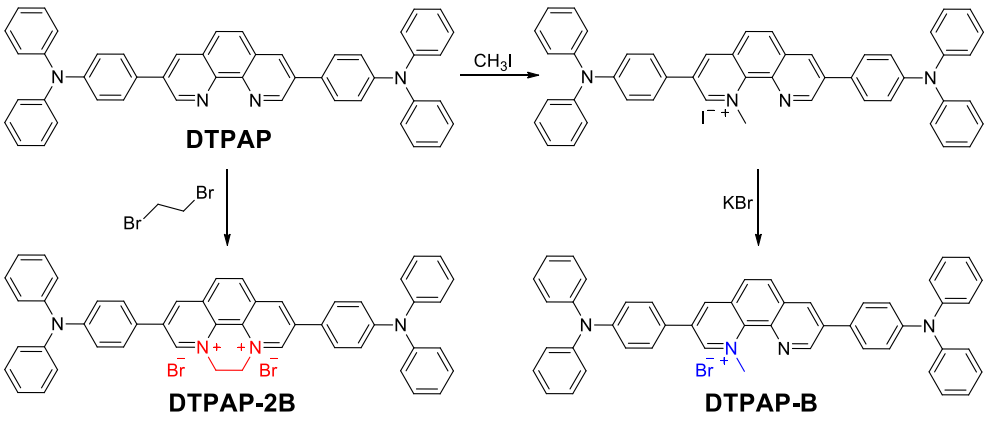

Scheme S1. Synthetic routes to DTPAP-B and DTPAP-2B.

Synthesis of DTPAP-B: To a two-neck flask (100 mL) was added DTPAP (667.5 mg, 0.5 mmol), CH_3I (199.2 mg, 0.6 mmol) and freshly distilled THF (10 mL). The reaction mixture was refluxed for 24 h. Then, the reaction was cooled to room temperature. The resulting slurry was suspended in CH_2Cl_2 (75 mL) and washed with H_2O (3×75 mL) followed by saturated aq. NH_4Cl (3×25 mL). The organic layer was collected, dried over Na_2SO_4, filtered, and concentrated under reduced pressure. The crude product was purified by silica gel column chromatography using CH_2Cl_2/MeOH (*v*: *v*, 50:1) as an eluent to afford a red solid (646 mg, 80% yield). In a 100 mL round bottom flask, the red solid was dissolved in methanol, excess sodium bromide was added, followed by extraction with CH_2Cl_2 and distilled water. Finally, the organic phases were separated and concentrated to give DTPAP-B (613 mg, 95% yield). ^{1}H NMR (600 MHz, DMSO-d_6) δ 9.84 (s, 1H), 9.53 (s, 2H), 8.90 (s, 1H), 8.31 (d, J = 22.9 Hz, 2H), 7.94 (d, J = 22.3 Hz, 4H), 7.40-7.37 (m, 8H), 7.16 – 7.11 (m, 16H), 5.31 (s, 3H). ^{13}C NMR (151 MHz, DMSO-d_6) δ 149.73, 149.53, 149.09, 147.97, 147.01, 146.86, 141.36, 139.09, 135.72, 135.57, 135.23, 133.12, 132.47, 132.03, 131.25, 130.32, 130.27, 129.09, 128.94, 128.31, 127.79, 125.84, 125.64, 125.54, 124.86, 124.62, 122.42, 122.20, 54.16. HRMS: m/z: $[M]^+$ calcd for $[C_{49}H_{37}N_4]^+$: 681.3018; found: 681.3026.

Synthesis of DTPAP-2B: To a 100 mL two-neck flask was added DTPAP (667.5 mg, 0.5 mmol), 1,2-dibromoethane (187.9 mg, 0.5 mmol) and freshly distilled THF (10 mL). The reaction mixture was refluxed for 24 h. After the reaction, the solution was filtered and the precipitate was washed with 80-100 mL of CH_2Cl_2 to obtain the target product DTPAP-2B in 90% yield. ^{1}H NMR (500 MHz, DMSO-d_6) δ 10.19 (s, 2H), 9.77 (s, 2H), 8.63 (s, 2H), 8.04 (d, J = 8.3 Hz, 4H), 7.43 (t, J = 7.9 Hz, 8H), 7.23-7.15 (m, 16H), 5.62 (s, 4H). ^{13}C NMR (151 MHz, DMSO-d_6) δ 150.43, 147.47, 146.59, 140.78, 138.09, 130.99, 130.44, 129.85, 129.49, 127.34, 126.02, 125.27, 125.21, 121.64, 52.59. HRMS: m/z: $[M]^{2+}$ calcd for $[C_{50}H_{40}N_4]^{2+}$: 347.1548; found: 347.1546.

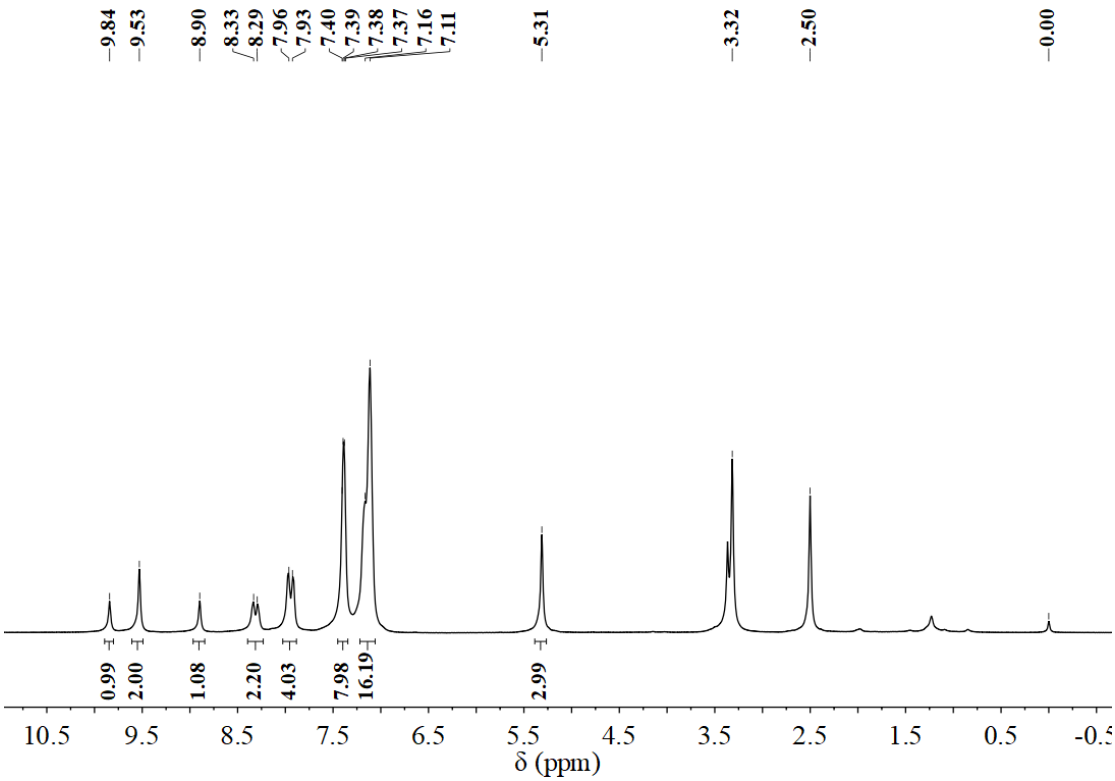

Figure S1. ^{1}H NMR spectrum of DTPAP-B in DMSO-d_6.

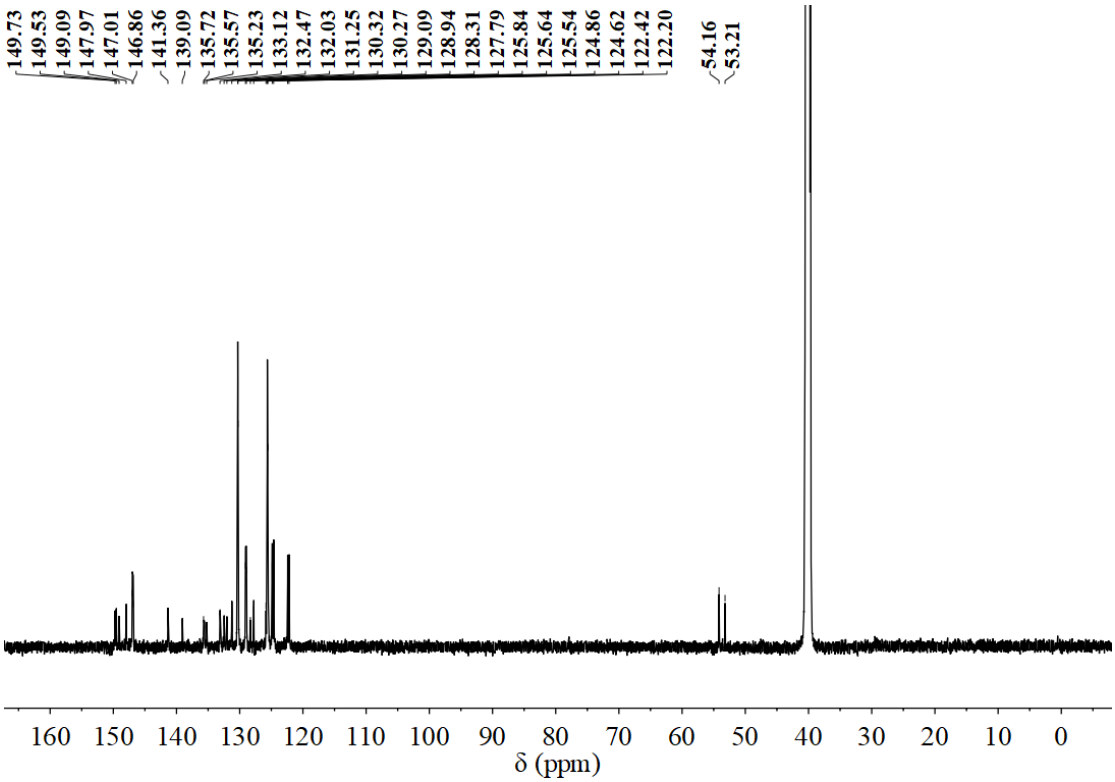

Figure S2. ^{13}C NMR spectrum of DTPAP-B in DMSO-d_6.

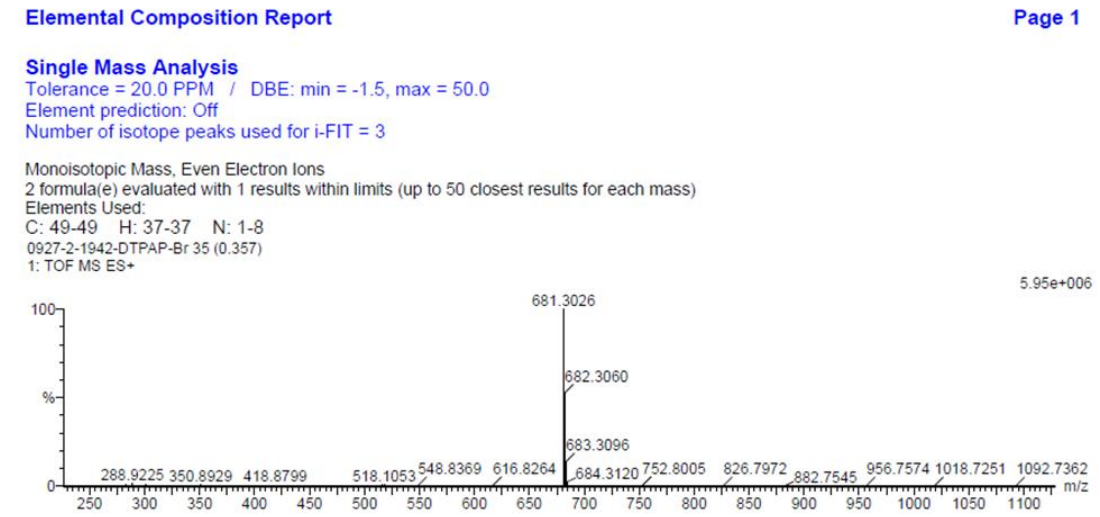

Figure S3. HRMS spectrum of DTPAP-B.

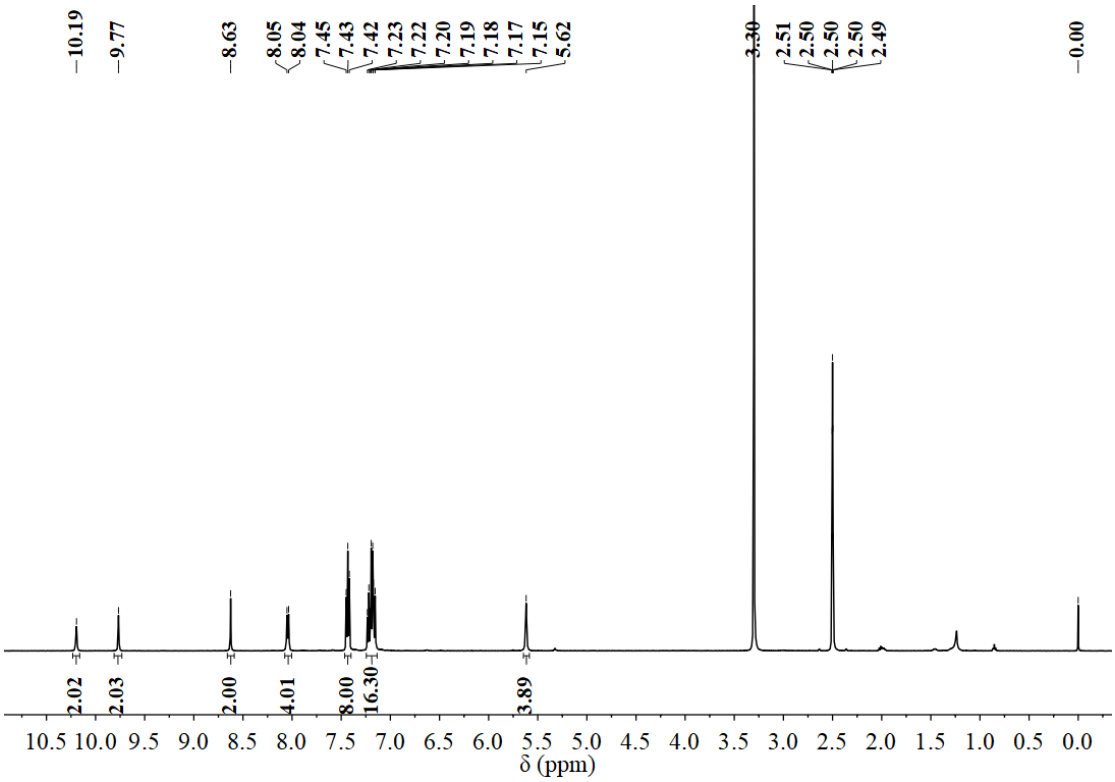

Figure S4. ^{1}H NMR spectrum of DTPAP-2B in DMSO-d_6.

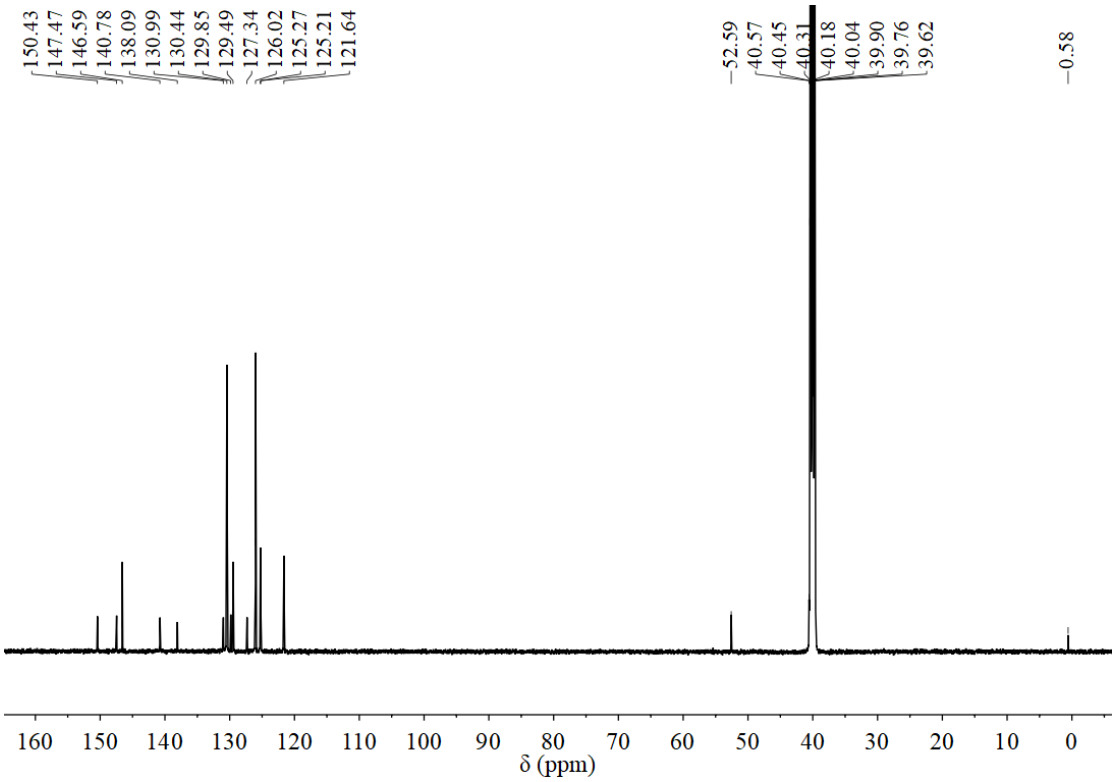

Figure S5. ^{13}C NMR spectrum of DTPAP-2B in DMSO-d_6.

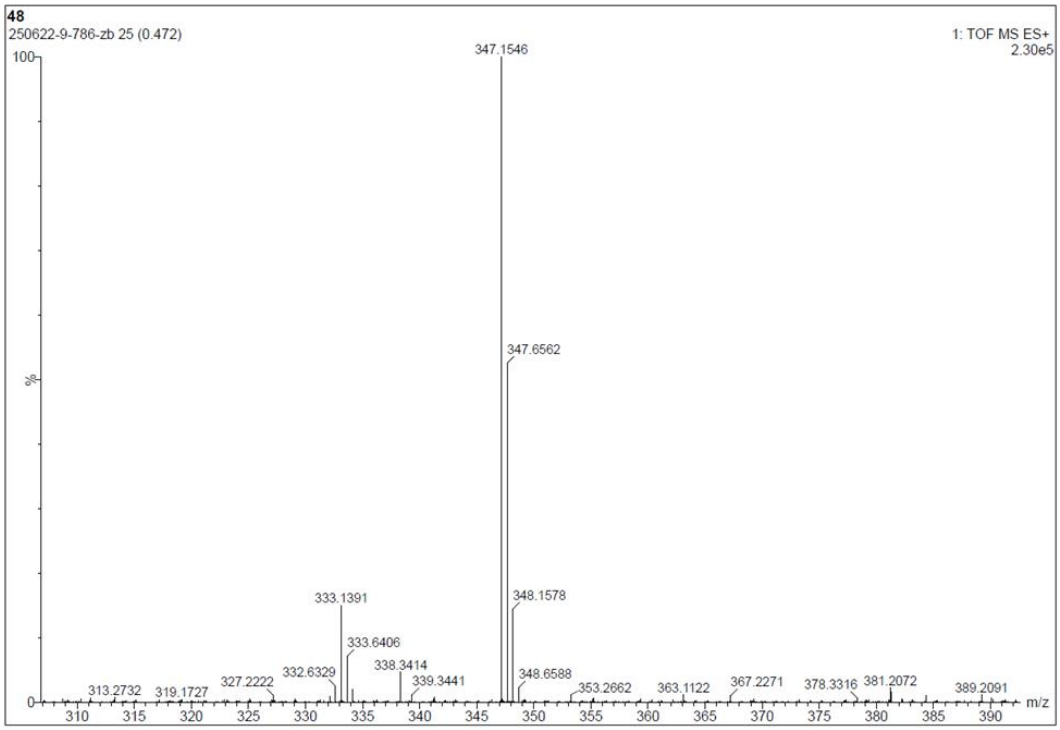

Figure S6. HRMS spectrum of DTPAP-2B.

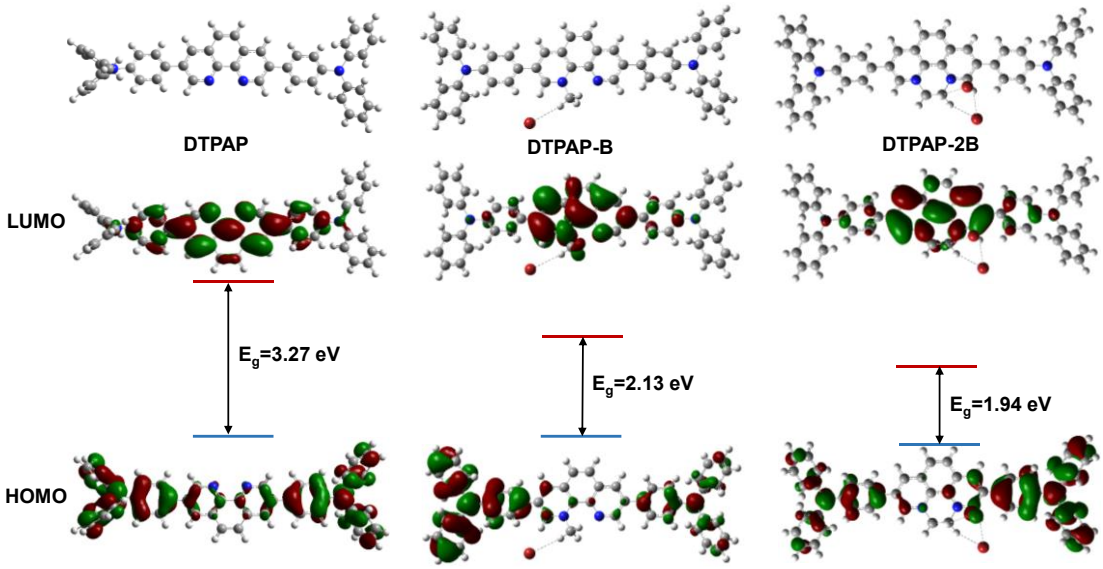

Figure S7. HOMO and LUMO electron cloud distribution of DTPAP, DTPAP-B and DTPAP-2B.

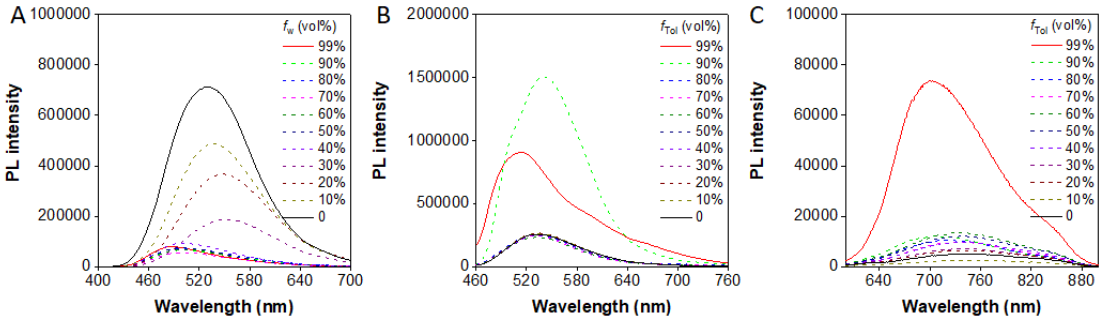

Figure S8. PL spectra of DTPAP (A) in DMSO/water mixtures with different water fractions (f_w). PL spectra of DTPAP-B (B) and DTPAP-2B (C) in DMSO/toluene mixtures with varied toluene fractions (f_{Tol}).

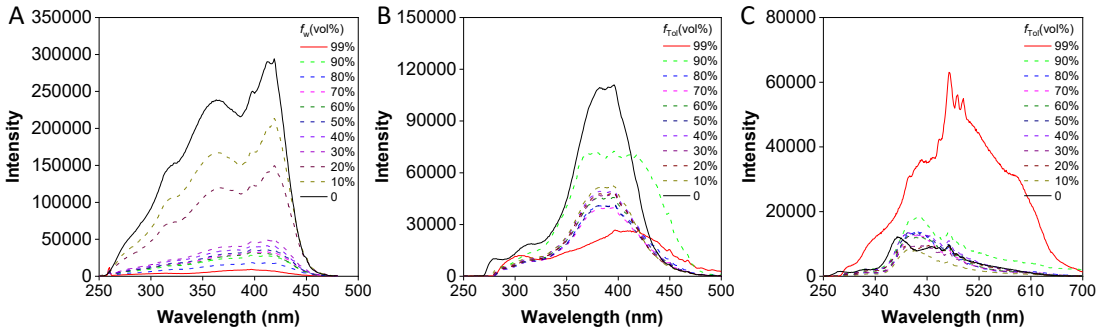

Figure S9. Excitation spectra of DTPAP (A) in DMSO/water mixtures with different f_w (DTPAP: Emission wavelength =520 nm, Excitation wavelength: 250-500 nm). DTPAP-B (B) and DTPAP-2B (C) in DMSO/toluene mixtures with f_{Tol} (DTPAP-B: Emission=560 nm, Excitation wavelength: 250-500 nm. DTPAP-2B: Emission=740 nm, Excitation wavelength: 250-700 nm).

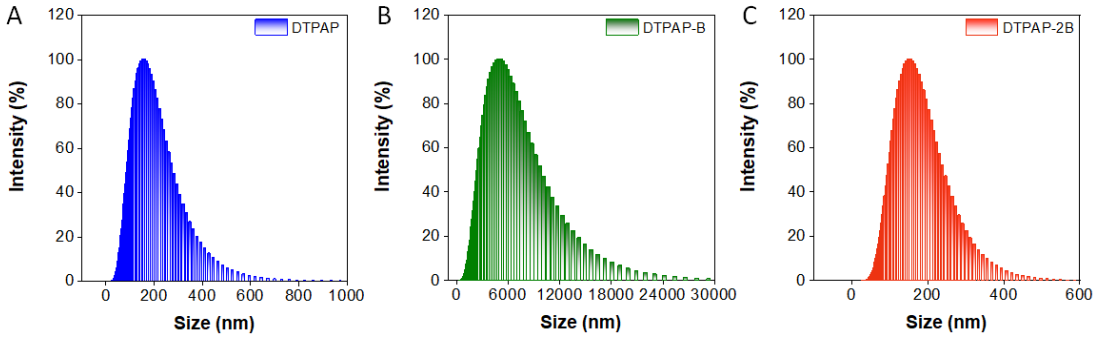

Figure S10. DLS of DTPAP in DMSO/water mixed solution with f_w of 99%. DLS of DTPAP-B and DTPAP-2B in DMSO/toluene mixed solution with f_{Tol} of 99%.

Table S1. Photophysical properties and excited-state decay rate of the three PSs.

	Sample	Φ_f (%)	τ_f (10^{-9} s)	k_r (10^7 s^{-1})	k_{nr} (10^8 s^{-1})
Solution[a]	DTPAP	93.94	3.66	25.67	0.17
	DTPAP-B	0.35	4.01	0.09	2.49
	DTPAP-2B	0.37	1.70	0.22	5.86
Aggregates	DTPAP[b]	3.73	1.66	2.25	5.80
	DTPAP-B[c]	3.39	2.98	1.14	3.24
	DTPAP-2B[c]	0.88	0.89	0.99	11.14

[a]Data were obtained in DMSO solution. [b]Data were measured in DMSO/H_2O mixed solution with H_2O fraction of 99%. [c]Data were measured in DMSO/toluene mixed solution with 99% toluene fraction. τ_f: average fluorescence lifetime calculated by $\tau_f = \Sigma(A_i\tau_i)^2/\Sigma A_i\tau_i$, where A_i is the pre-exponential for lifetime τ_i. Φ_f = fluorescence quantum yield measured by using an integrating sphere. k_r = radiative decay rate (Φ_f/τ_f). k_{nr} = nonradiative decay rate ($1/\tau_f - k_r$).

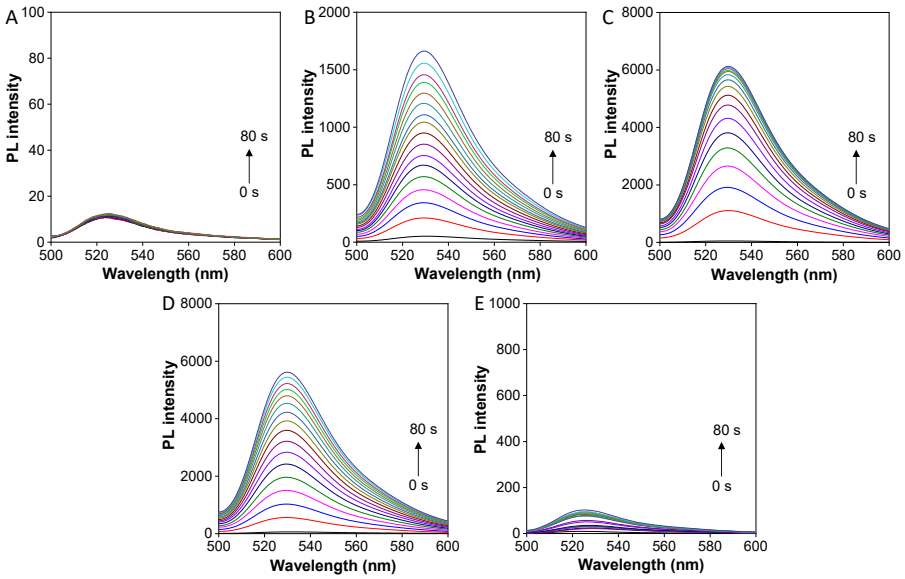

Figure S11. The fluorescence spectra change of DCFH in the presence of (A) DCFH alone, (B) DTPAP, (C) DTPAP-B, (D) DTPAP-2B and (E) RB (0.25 μM) upon different time of white light (10 mW cm^{-2}) irradiation.

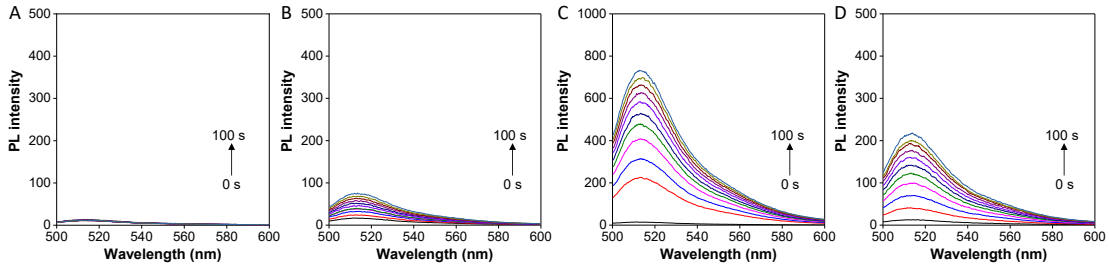

Figure S12. The fluorescence spectra change of APF in the presence of (A) APF alone, (B) DTPAP, (C) DTPAP-B and (D) DTPAP-2B (0.25 μM) upon different time of white light (10 mW cm^{-2}) irradiation.

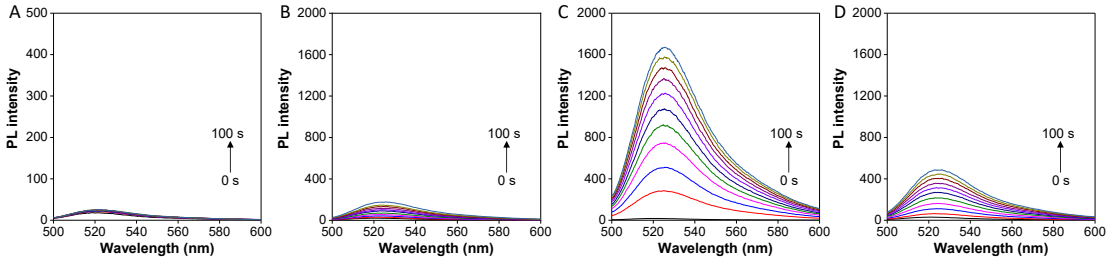

Figure S13. The fluorescence spectra change of DHR123 in the presence of (A) DHR123 alone, (B) DTPAP, (C) DTPAP-B and (D) DTPAP-2B (0.25 μM) upon different time of white light (10 mW cm^{-2}) irradiation.

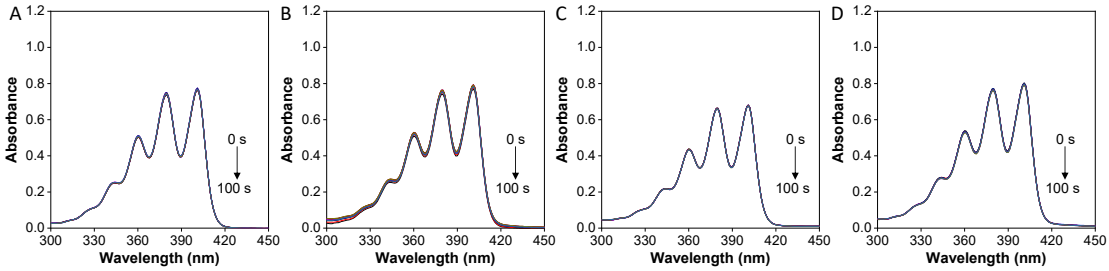

Figure S14. The absorption spectra change of ABDA in the presence of (A) ABDA alone, (B) DTPAP, (C) DTPAP-B and (D) DTPAP-2B (0.25 μM) upon different time of white light (10 mW cm^{-2}) irradiation.

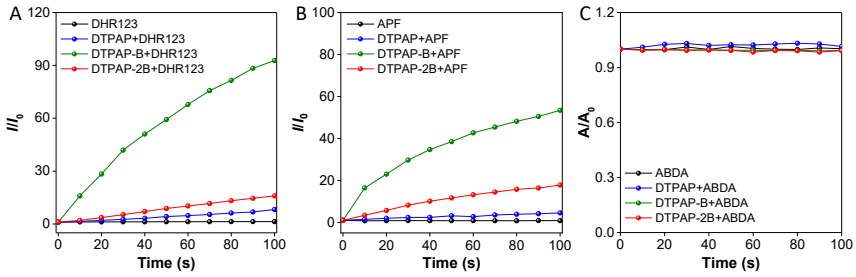

Figure S15. Relative PL intensity of (A) DHR123 and (B) APF and changes in relative absorbance of (C) ABDA in the absence or presence of DTPAP, DTPAP-B or DTPAP-2B after being irradiated with white light (10 mW cm^{-2}).

Table S2. Crystallographic and structural refinement data of DTPAP-2B, DTPAP-B and DTPAP.

Name	DTPAP-2B[a]	DTPAP-B[b]	DTPAP[c]
Empirical formula	$C_{54}H_{54}Br_2N_4O_4$	$C_{57}H_{54}Br_{0.92}N_4O_4$	$C_{49}H_{35}Cl_3N_4$
Formula weight	982.83	932.52	786.16
Temperature (K)	220(2)	153(2)	120.00(10)
Crystal system	monoclinic	monoclinic	triclinic
Crystal size/mm^3	0.14 × 0.11 × 0.09	0.15 × 0.12 × 0.1	0.16 × 0.13 × 0.09
Space group	$P2_1/n$	P2/c	P-1
a (Å)	11.0375(6)	20.1429(11)	10.2442(2)
b (Å)	8.4725(5)	10.8615(5)	10.4061(3)
c (Å)	48.750(4)	22.1765(14)	19.7416(5)
α (°)	90	90	85.184(2)
β (°)	90.538(7)	109.655(7)	80.187(2)
γ (°)	90	90	68.756(2)
Volume (Å^3)	4558.7(5)	4569.1(5)	1932.23(9)
Z	4	4	2
2θ range for data collection (°)	3.63 to 73.65	4.658 to 133.196	9.1 to 136.5
Index ranges	$-12 \le h \le 13$, $-7 \le k \le 10$, $-40 \le l \le 60$	$-23 \le h \le 23$, $-12 \le k \le 10$, $-19 \le l \le 26$	$-12 \le h \le 10$, $-12 \le k \le 12$, $-23 \le l \le 23$
Reflections collected	20195	17762	18697
Final R indexes [I>=2σ (I)]	$R_1 = 0.0605$, $wR_2 = 0.1427$	$R_1 = 0.0837$, $wR_2 = 0.2380$	$R_1 = 0.0425$, $wR_2 = 0.1123$
Final R indexes [all data]	$R_1 = 0.0836$, $wR_2 = 0.1580$	$R_1 = 0.1078$, $wR_2 = 0.2662$	$R_1 = 0.0496$, $wR_2 = 0.1167$
Independent reflections	8940 [$R_{int} = 0.0526$, $R_{sigma} = 0.0701$]	8062 [$R_{int} = 0.0509$, $R_{sigma} = 0.0565$]	6937 [$R_{int} = 0.0373$, $R_{sigma} = 0.0376$]
Data/restraints/parameters	8940/12/526	8062/145/507	6937/0/505
Goodness-of-fit on F^2	1.033	1.058	1.030

[a]CCDC: 2387016. [b]CCDC: 2387022. [c]CCDC:2524304. These data can be obtained free of charge via the joint Cambridge Crystallographic Data Centre (CCDC) and Fachinformationszentrum Karlsruhe Access Structures service.

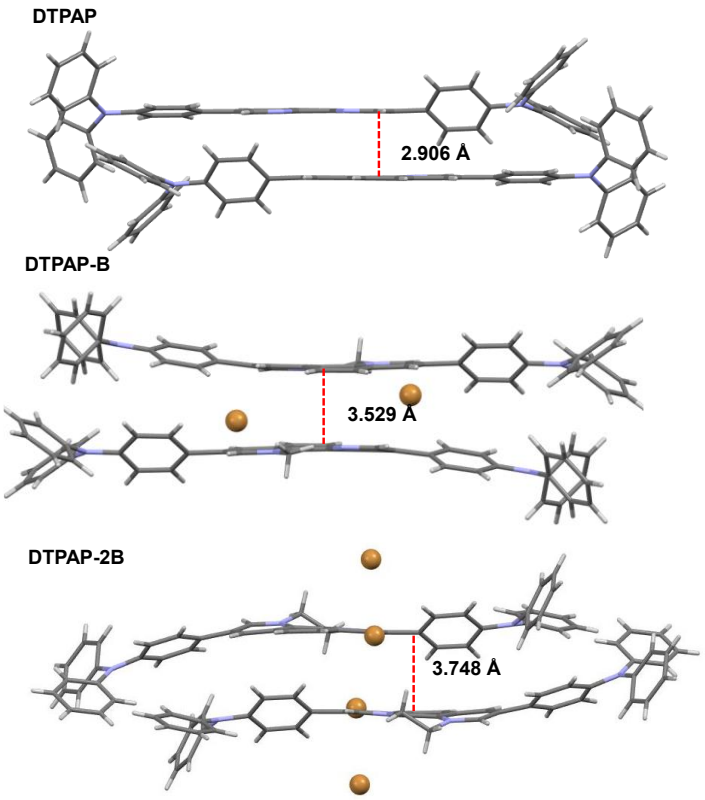

Figure S16. Single-crystal X-ray diffraction analysis. Molecular packing and Interlayer dimer structure diagrams of DTPAP, DTPAP-B, and DTPAP-2B single crystals.

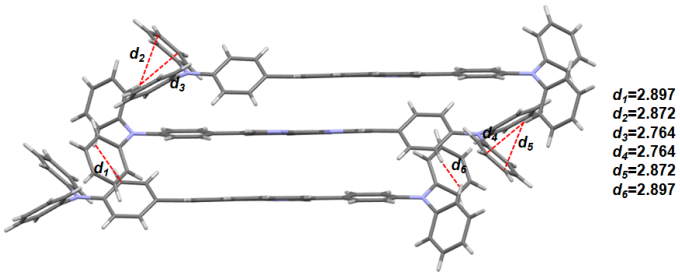

Figure S17. Single crystal structure, interlayer structure, and monolayer molecular interactions of DTPAP.

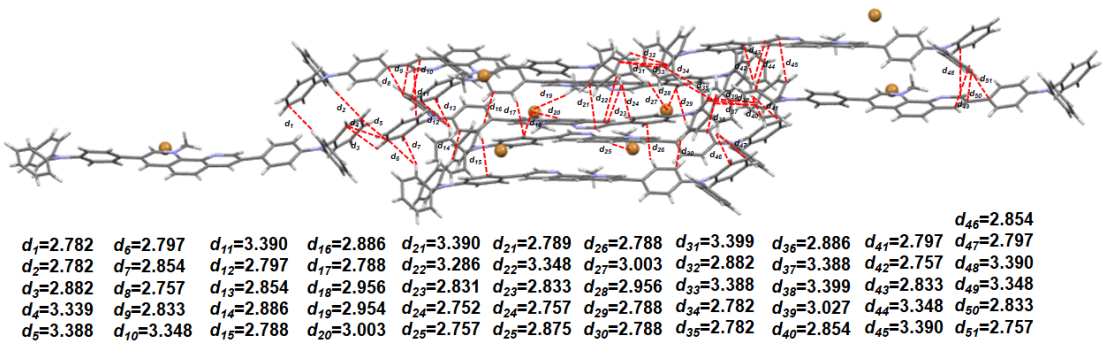

Figure S18. Single crystal structure, interlayer structure, and monolayer molecular interactions of DTPAP-B.

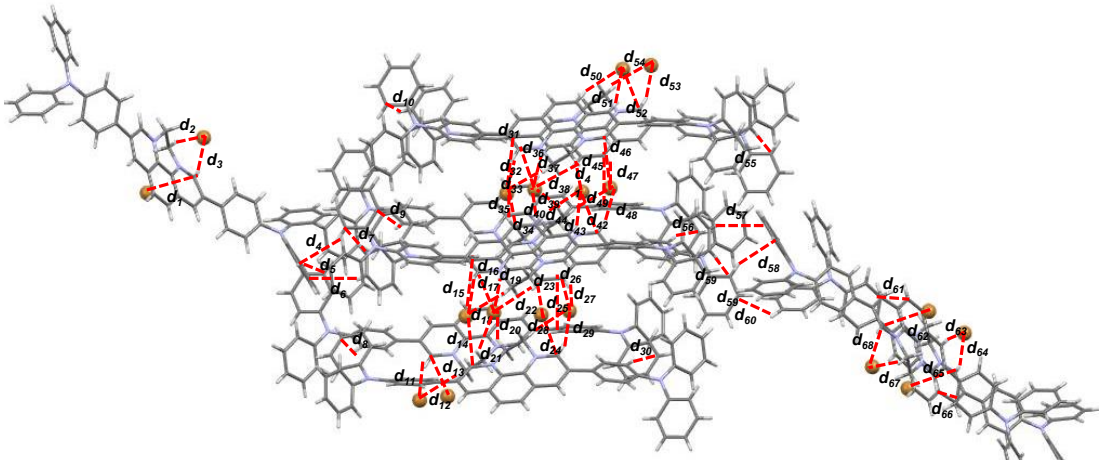

d_1=3.525	d_6=2.871	d_{11}=2.839	d_{16}=2.839	d_{21}=2.987	d_{26}=3.409	d_{31}=3.351	d_{36}=3.525
d_2=2.755	d_7=2.677	d_{12}=2.755	d_{17}=3.525	d_{22}=2.853	d_{27}=2.862	d_{32}=2.839	d_{37}=2.895
d_3=2.839	d_8=2.788	d_{13}=3.525	d_{18}=2.755	d_{23}=2.897	d_{28}=2.755	d_{33}=2.755	d_{38}=2.853
d_4=2.833	d_9=2.788	d_{14}=3.409	d_{19}=2.895	d_{24}=3.525	d_{29}=2.839	d_{34}=3.409	d_{39}=2.897
d_5=2.833	d_{10}=2.677	d_{15}=3.351	d_{20}=2.897	d_{25}=3.351	d_{30}=2.788	d_{35}=2.862	d_{40}=2.987

d_{41}=2.897	d_{46}=3.409	d_{51}=2.895	d_{56}=2.788	d_{61}=3.351	d_{66}=3.525
d_{42}=3.525	d_{47}=2.862	d_{52}=3.525	d_{57}=2.872	d_{62}=3.525	d_{67}=2.755
d_{43}=2.895	d_{48}=2.839	d_{53}=2.839	d_{58}=2.833	d_{63}=2.755	d_{68}=2.839
d_{44}=2.853	d_{49}=2.755	d_{54}=2.755	d_{59}=2.677	d_{64}=2.839	
d_{45}=3.351	d_{50}=2.853	d_{55}=2.677	d_{60}=2.871	d_{65}=3.351	

Figure S19. Single crystal structure, interlayer structure, and monolayer molecular interactions of DTPAP-2B.

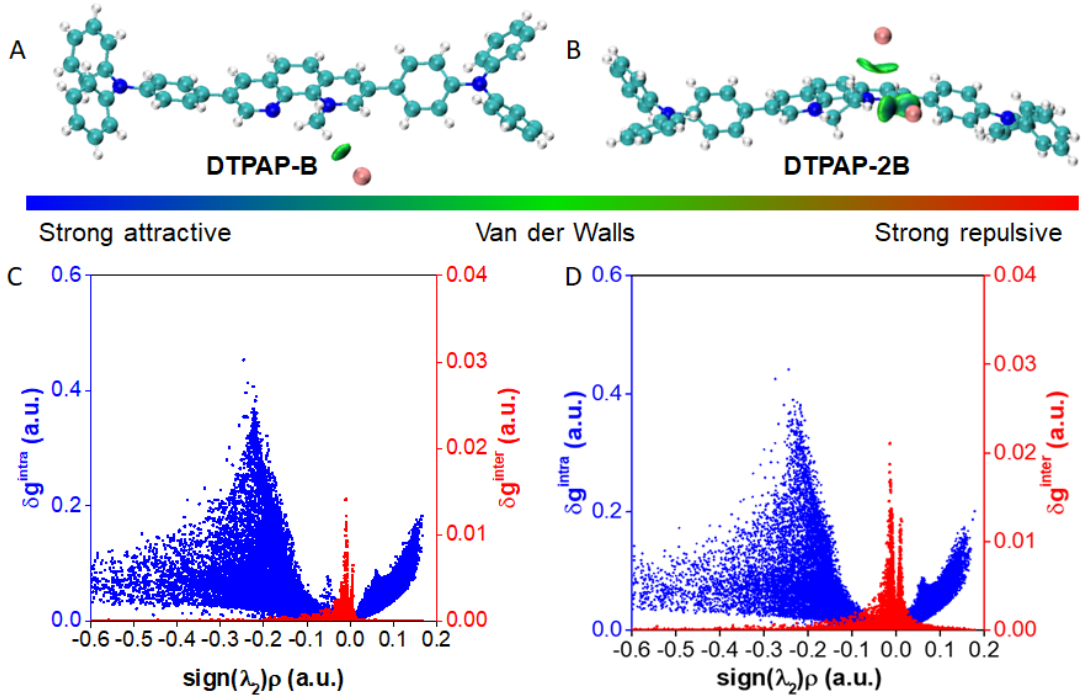

Figure S20. The visualized isosurfaces of the IGM analysis for monomer in (A) DTPAP-B or (B) DTPAP-2B (δg_{inter} = 0.007). The 2D plot of δg_{intra} (blue) and δg_{inter} (red) for (C) DTPAP-B and (D) DTPAP-2B.

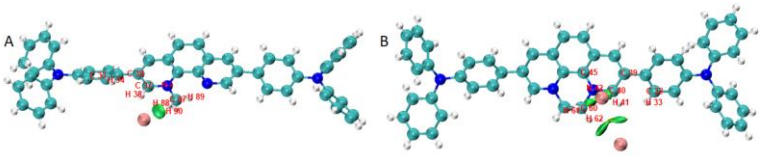

Atomic pair	Delta-g index	Percentage contribution
1 88	0.121877	38.60 %
1 87	0.061383	19.44 %
1 38	0.035675	11.30 %
1 37	0.022968	7.27 %
1 90	0.016788	5.32 %
1 89	0.014697	4.66 %
1 34	0.011815	3.74 %
1 2	0.011256	3.57 %
1 33	0.006107	1.93 %
1 39	0.003682	1.17 %

Atomic pair	Delta-g index	Percentage contribution
1 62	0.161234	11.60 %
1 42	0.144500	10.40 %
2 40	0.110711	7.96 %
2 61	0.096814	6.97 %
1 60	0.088863	6.39 %
1 40	0.087148	6.27 %
2 60	0.083282	5.99 %
2 4	0.077590	5.58 %
1 33	0.056989	4.10 %
2 41	0.053049	3.82 %

Figure S21. The calculated contribution of ten atomic pairs with the largest percentage to interactions between the π^+ core and bromine ions in (A) DTPAP-B and (B) DTPAP-2B.

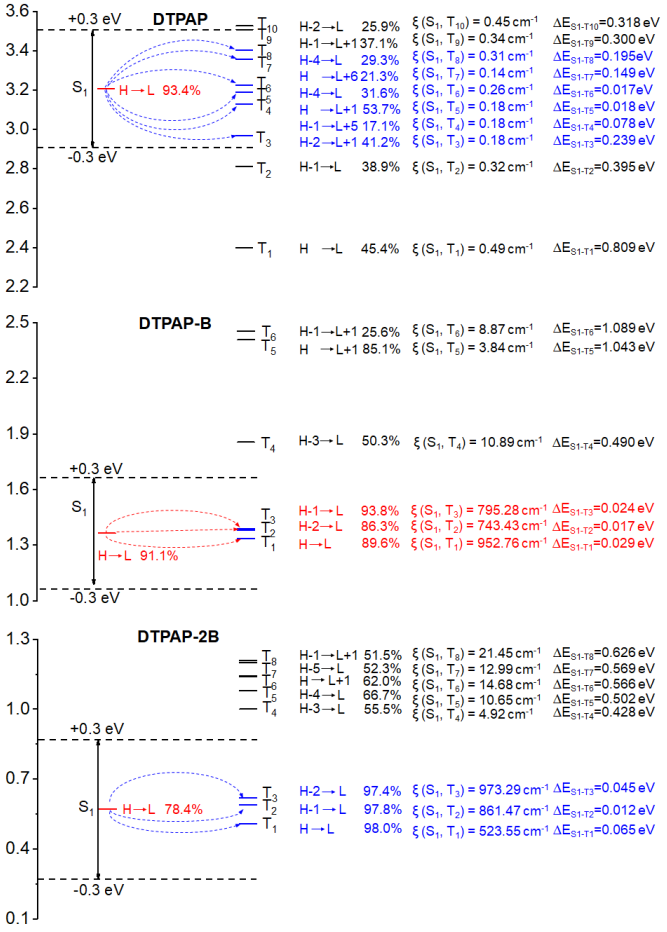

Figure S22. Schematic diagrams showing the TD-DFT-calculated energy levels, ISC channels, SOC constants (ξ) as well as energy gaps ($\Delta E_{S1\text{-}Tn}$) between S_1 and T_n of DTPAP, DTPAP-B and DTPAP-2B at singlet (S_n) and triplet (T_n) states. Note that H and L refer to highest occupied molecular orbital and lowest unoccupied molecular orbital, respectively. The red and blue dashed arrows represent the intersystem crossing processes probably occurring from the S_1 state to its higher- or lower-lying triplet states (T_n). The blue lines refer to the triplet states available for effective intersystem crossing transitions.

Table S3. The S_1 and T_n state transition configurations of DTPAP, DTPAP-B and DTPAP-2B revealed by TD-DFT calculations.

		Energy level	Transition configuration
DTPAP	S_1	3.21	H → L 93.4%
	T_1	2.40	H → L 45.4%, H-2 → L+1 13.8%, H-3 → L 12.0%, H-1 → L 8.0%,
	T_2	2.81	H-1 → L 38.9%, H → L+2 20.2%, H-2 → L+1 10.4%
	T_3	2.97	H-2 → L+1 41.2%, H → L 17.8%, H-1 → L+2 9.4%
DTPAP-B	S_1	1.36	H → L 91.1%, H-2 → L 5.3%
	T_1	1.34	H → L 89.6%, H-2 → L 6.1%
	T_2	1.38	H-2 → L 86.3%, H → L 5.9%
	T_3	1.39	H-1 → L 93.8%
DTPAP-2B	S_1	0.58	H → L 78.4%, H-1 → L 18.5%
	T_1	0.51	H → L 98.0%
	T_2	0.59	H-1 → L 97.8%
	T_3	0.62	H-2 → L 97.4%

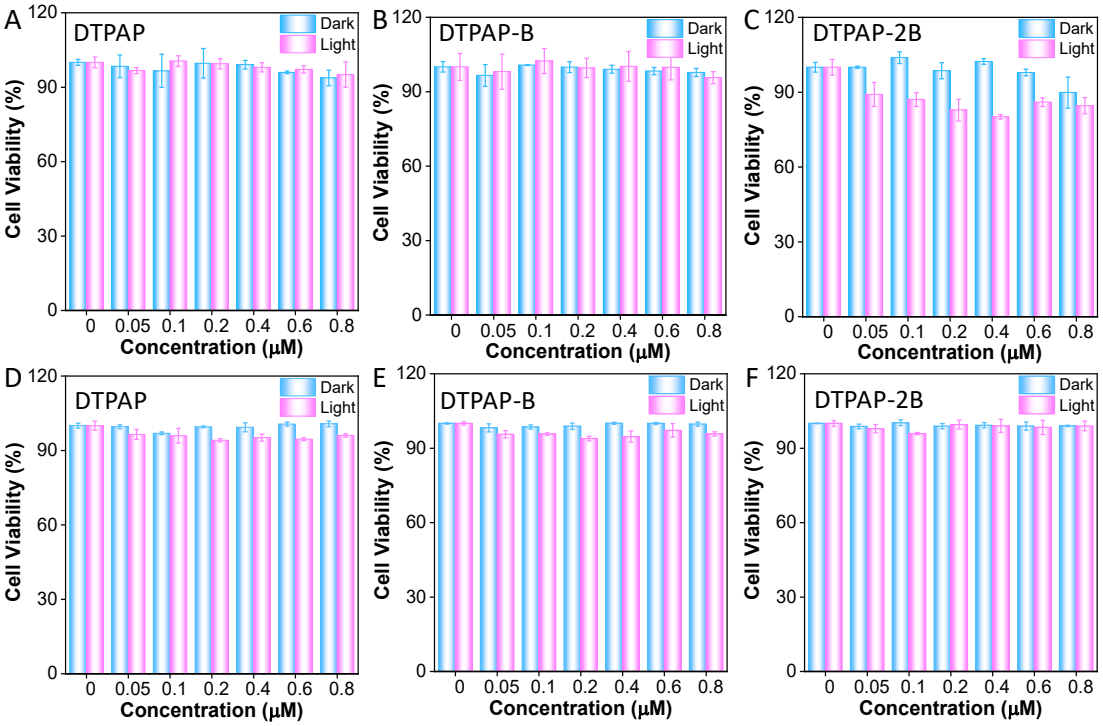

Figure S23. Viability of LO2 cells (A-C) and NIH3T3 cells (D-E) incubated with various concentrations of DTPAP, DTPAP-B or DTPAP-2B with/without white light (100 mW cm^{-2}).

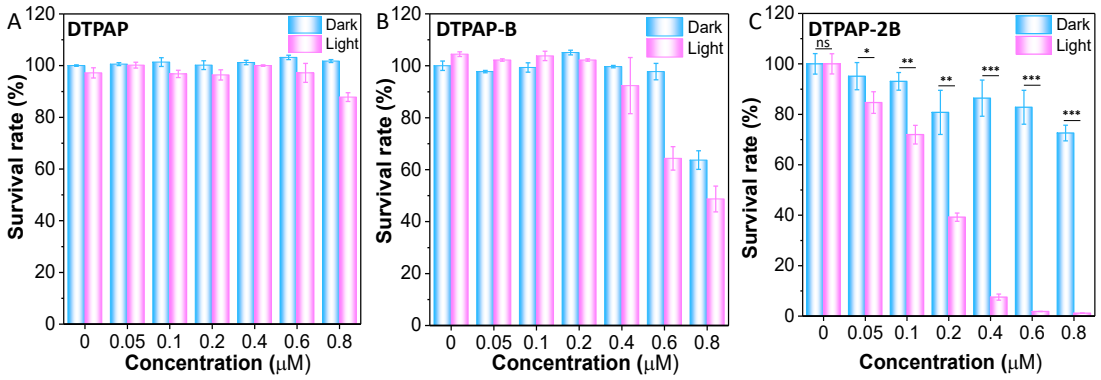

Figure S24. Bacteria survival rates of *S. aureus* exposed to DTPAP (A), DTPAP-B (B) or DTPAP-2B (C) of varied concentrations in darkness or under white light irradiation (100 mW cm^{-2}) (n = 3, *p<0.05, **p<0.01, ***p<0.001).

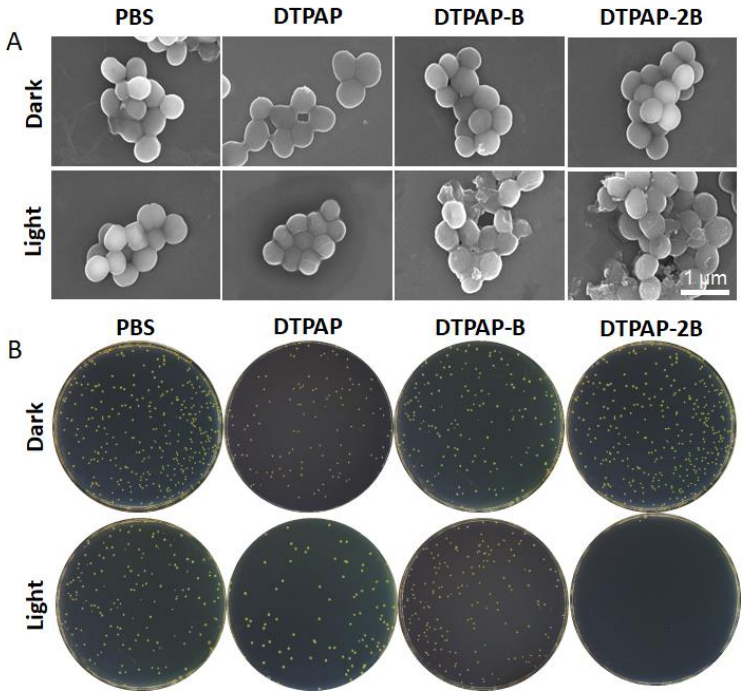

Figure S25. (A) SEM images of *S. aureus* incubated with PBS, DTPAP, DTPAP-B or DTPAP-2B for 15 min, then stayed in darkness or under white light irradiation (100 mW cm^{-2}) for 15 min. (B) Photographs of *S. aureus* treated with DTPAP, DTPAP-B or DTPAP-2B on the agar plates under darkness or light conditions.

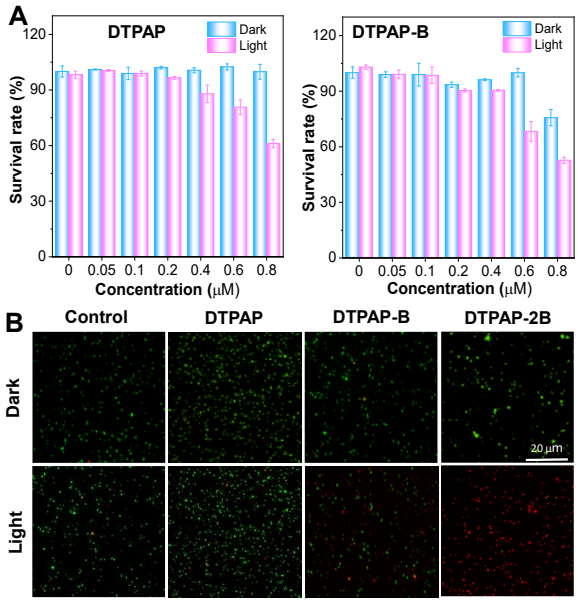

Figure S26. (A) Survival rate of MRSA incubated with DTPAP or DTPAP-B of varied concentrations in darkness or under white light irradiation (100 mW cm^{-2}). (B) Live/dead bacterial staining images of MRSA treated with PBS, DTPAP, DTPAP-Br or DTPAP-2Br with/without white light irradiation. Green channel: Calcein-AM. Red channel: propidium iodide. Scale bar = 20 μm.

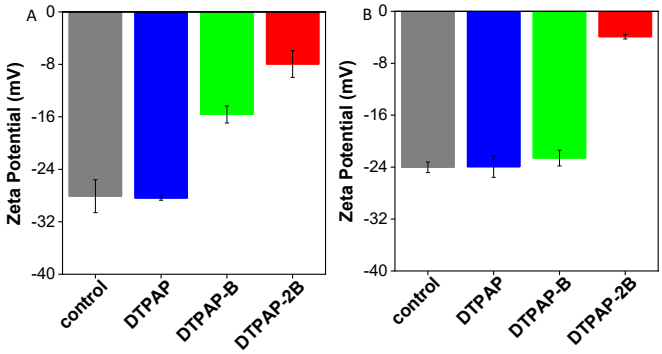

Figure S27. The zeta potential of *S. aureus* (A) and MRSA (B) incubated with DTPAP, DTPAP-B or DTPAP-2B (50 μM).

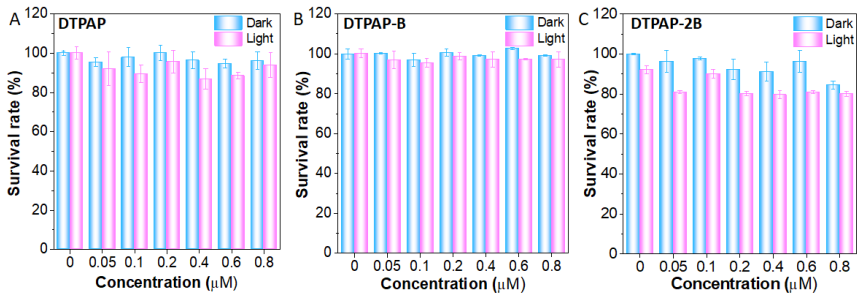

Figure S28. Bacteria survival rates of *E. coli* treated with DTPAP (A), DTPAP-B (B) or DTPAP-2B (C) of varied concentrations in darkness or under white light irradiation (100 mW cm^{-2}).

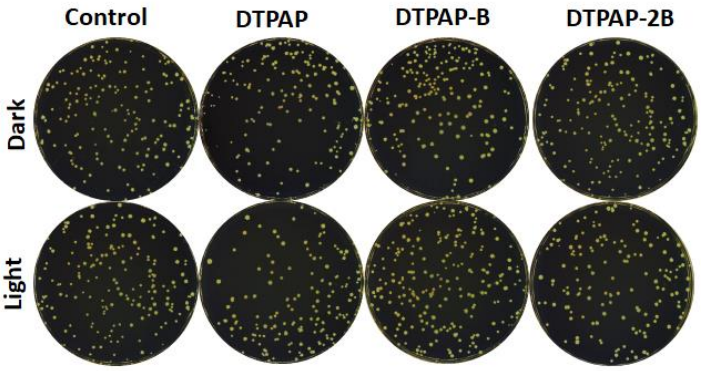

Figure S29. Photographs of *E. coli* cultured on an agar plate after being treated with PBS, DTPAP, DTPAP-B or DTPAP-2B (0.8 μM).

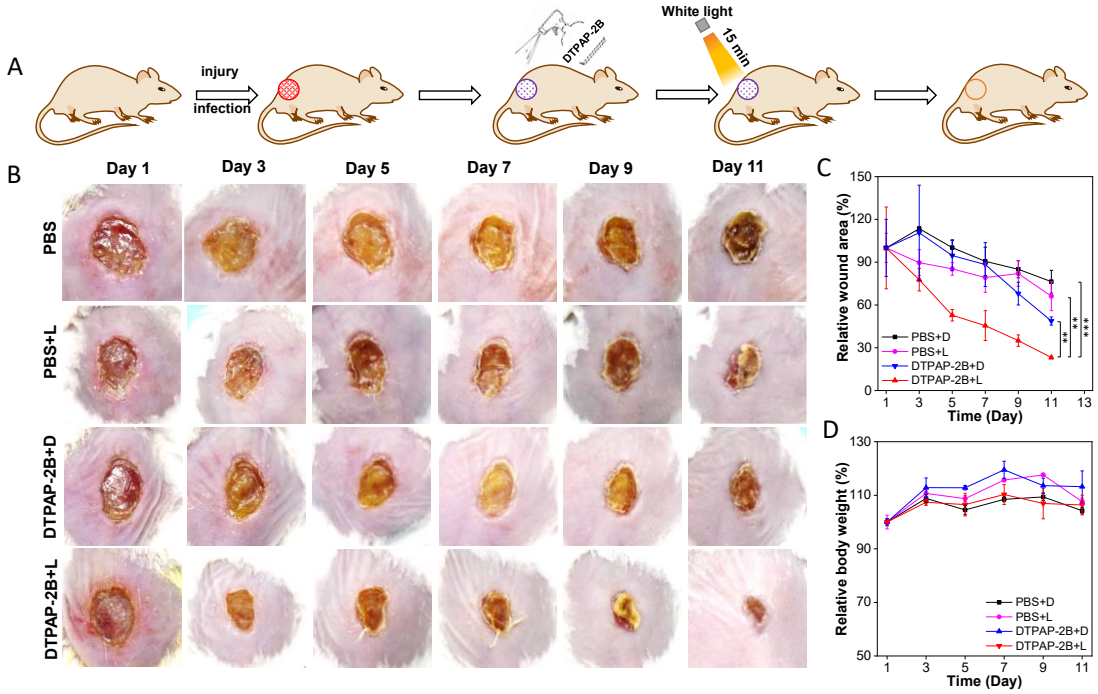

Figure S30. (A) Schematics of the photodynamic anti-infection of MRSA-infected wound model with DTPAP-2B. (B) Photographs of MRSA-infected wounds after treatment with PBS or DTPAP-2B (50 μM) with or without white light irradiation (100 mW cm^{-2}). (C) The relative wound area during the wound healing process. Data were presented as mean ± SD (n = 3, ***p<0.001, **p<0.01). (D) The relative body weight during the wound healing process.

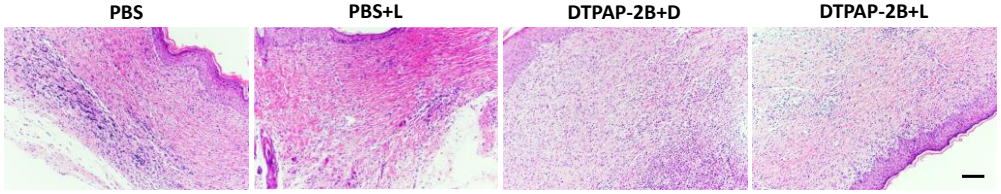

Figure S31. H&E staining images of wound tissues after treatment for 11 days, obtained from a 5 mm × 5 mm area encompassing the wound edge and adjacent dorsal tissue of the mouse. Scale bar = 20 μm.

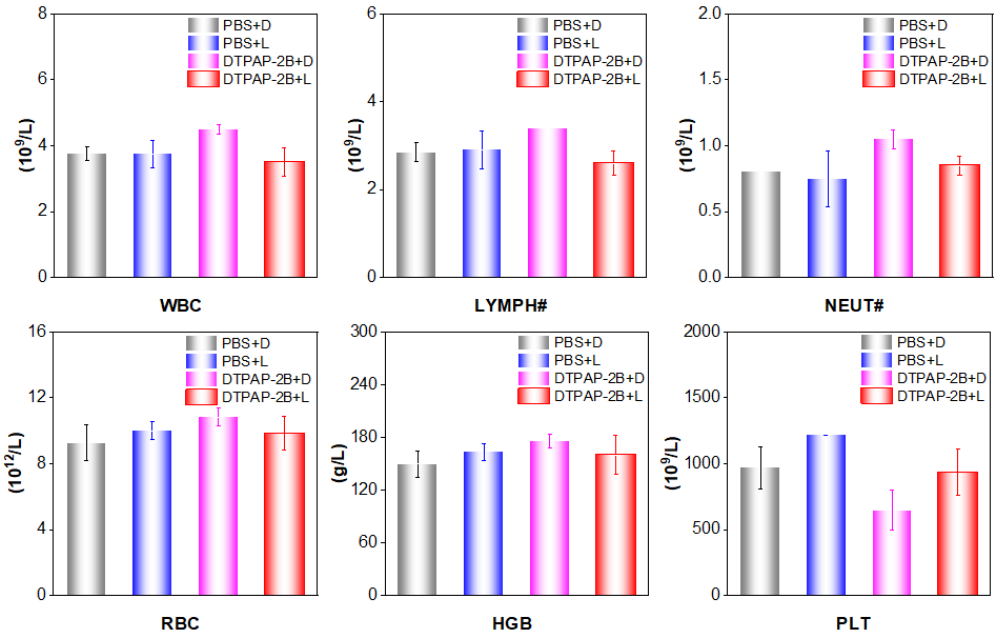

Figure S32. Blood routine assays of MRSA-infected mice at day 11 after different treatments.

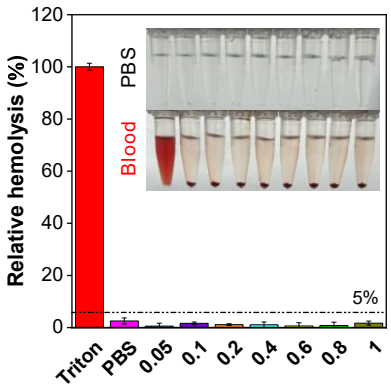

Figure S33. Hemolysis rates of DTPAP-2B. Triton and PBS were used as the positive control and negative control, respectively. Inset: the photographs of hemolytic activity.

References

[S1] M. J. Frisch, G. W. Trucks, H. B. Schlegel, G. E. Scuseria, M. A. Robb, J. R. Cheeseman, G. Scalmani, V. Barone, B. Mennucci, G. A. Petersson, H. Nakatsuji, M. Caricato, X. Li, H. P. Hratchian, A. F. Izmaylov, J. Bloino, G. Zheng, J. L. Sonnenberg, M. Hada, M. Ehara, K. Toyota, R. Fukuda, J. Hasegawa, M. Ishida, T. Nakajima, Y. Honda, O. Kitao, H. Nakai, T. Vreven, J. A. Montgomery Jr, J. E. Peralta, F. Ogliaro, M. J. Bearpark, J. Heyd, E. N. Brothers, K. N. Kudin, V. N. Staroverov, R. Kobayashi, J. Normand, K. Raghavachari, A. P. Rendell, J. C. Burant, S. S. Iyengar, J. Tomasi, M. Cossi, N. Rega, N. J. Millam, M. Klene, J. E. Knox, J. B. Cross, V. Bakken, C. Adamo, J. Jaramillo, R. Gomperts, R. E. Stratmann, O. Yazyev, A. J. Austin, R. Cammi, C. Pomelli, J. W. Ochterski, R. L. Martin, K. Morokuma, V. G. Zakrzewski, G. A. Voth, P. Salvador, J. J. Dannenberg, S. Dapprich, A. D. Daniels, Ö. Farkas; J. B. Foresman, J. V. Ortiz, J. Cioslowski, D. J. Fox, Gaussian 09, Revision D.01, Gaussian, Inc.: Wallingford, CT, (2009).

[S2] Y. Zhao, D.G. Truhlar, The M06 suite of density functionals for main group thermochemistry, thermochemical kinetics, noncovalent interactions, excited states, and transition elements: two new functionals and systematic testing of four M06-class functionals and 12 other functionals, Theor. Chem. Acc. 120 (2008) 215-241.

[S3] G.W.T. M. J. Frisch, H. B. Schlegel, G. E. Scuseria, J. R. C. M. A. Robb, G. Scalmani, V. Barone, B. Mennucci, H. N. G. A. Petersson, M. Caricato, X. Li, H. P. Hratchian, J. B. A. F. Izmaylov, G. Zheng, J. L. Sonnenberg, M. Hada, K. T. M. Ehara, R. Fukuda, J. Hasegawa, M. Ishida, T. Nakajima, O. K. Y. Honda, H. Nakai, T. Vreven, J. A. Montgomery Jr, F. O. J. E. Peralta, M. Bearpark, J. J. Heyd, E. Brothers, V. N. S. K. N. Kudin, T. Keith, R. Kobayashi, J. Normand, A. R. K. Raghavachari, J. C. Burant, S. S. Iyengar, J. Tomasi, N. R. M. Cossi, J. M. Millam, M. Klene, J. E. Knox, J. B. Cross, C. A. V. Bakken, J. Jaramillo, R. Gomperts, R. E. Stratmann, A. J. A. O. Yazyev, R. Cammi, C. Pomelli, J. W. Ochterski, K. M. R. L. Martin, V. G. Zakrzewski, G. A. Voth, J. J.D. P. Salvador, S. Dapprich, A. D. Daniels, J. B. F. O. Farkas, J. V. Ortiz, J. Cioslowski, D. J. Fox, Gaussian 09, Revision D.01, Gaussian Inc. Wallingford CT, (2013).

[S4] F. Neese, F. Wennmohs, U. Becker, C. Riplinger, The ORCA quantum chemistry program package, J. Chem. Phys. 152 (2020) 224108.

[S5] A. D. W. Humphrey, K. Schulten, J. Mol. Graphics. 14 (1996) 33-38.

[S6] Rigaku Oxford Diffraction. CrysAlisPRO Software System, Version 1.171.38.43f; Rigaku Corporation: Oxford, UK, (2015).

[S7] G.M Sheldrick, Acta Cryst. A 64 (2008) 112-122.

[S8] G. M. Sheldrick, Crystal structure refinement with SHELXL. Acta Cryst. C71 (2015) 3-8.

[S9] O. V. Dolomanov, L. J. Bourhis, R. J. Gildea, J. A. K. Howard, H. Puschmann, OLEX2: a complete structure solution, refinement and analysis program. J. Appl. Crystallogr. 42 (2009) 339-341.

[S10] L. J. Bourhis, O. V. Dolomanov, R. J. Gildea, J. A. K. Howard, H. Puschmann, The anatomy of a comprehensive constrained, restrained refinement program for the modern computing environment-Olex2 dissected. Acta Cryst. A 71 (2015) 59-75.

[S11] M. Louis, H. Thomas, M. Gmelch, A. Haft, F. Fries, S. Reineke, Blue-light-absorbing thin films showing ultralong room-temperature phosphorescence, Adv. Mater. 31 (2019) 1807887.